


## Article

# Body Morphology and Drag in Swimming: CFD Analysis of the Effects of Differences in Male and Female Body Types

Andrew X. G. Wang<sup>1,\*</sup> and Zbigniew J. Kabala<sup>2</sup> <sup>1</sup> Pioneer Academics, 30 S 15th St, 15th Floor, Philadelphia, PA 19102, USA<sup>2</sup> Department of Civil & Environmental Engineering, Duke University, Durham, NC 27708, USA

\* Correspondence: andwang@ctemc.org

**Abstract:** This study analyzes the effect of the morphological characteristics of swimmers on passive drag and determines whether the female or male body type is more efficient for gliding. As a result of puberty, males and females develop different body structures; this study investigates whether these changes in shape influence drag. Computational fluid dynamics (CFD) simulations carried out in Ansys Fluent software were used to calculate the drag force and coefficient from 2D models of swimmers in streamline position, generated based on common anthropometric measurements. Both the top and side view profiles of the swimmers were simulated, unique to this study. The normalized male and female body shapes were simulated at different velocities, and it was demonstrated that the male body shape has a lower drag coefficient than the female body shape by 10.1% and 2.8% for top view and side view profiles, respectively. The in-depth analysis and simulation of models with varying hip and chest dimensions found a significant and positive correlation between hip and chest size and drag, with the chest size having the largest effect of an average 12.2% increase in drag per 5% increase in chest breadth. The results from modifying anthropometric variables explain the discrepancy between the drag experienced by male and female swimmers and show that enlarged hips and chests cause an increase in resistance. The differences between drag for males and females were found to be comparable to the 6.2% and 7.7% drag differences between full-body fastskin and normal suits, indicating measurable impact on performance. These findings suggest that the morphology of swimmers does have a significant effect on drag and that the male body shape is more hydrodynamic than the female body shape.

**Keywords:** computational fluid dynamics (CFD); drag coefficient; swimming; body morphology; streamline; male and female body type comparison



**Citation:** Wang, A.X.G.; Kabala, Z.J. Body Morphology and Drag in Swimming: CFD Analysis of the Effects of Differences in Male and Female Body Types. *Fluids* **2022**, *7*, 332. <https://doi.org/10.3390/fluids7100332>

Academic Editor: Mehrdad Massoudi

Received: 23 August 2022

Accepted: 12 October 2022

Published: 19 October 2022

**Publisher's Note:** MDPI stays neutral with regard to jurisdictional claims in published maps and institutional affiliations.



**Copyright:** © 2022 by the authors. Licensee MDPI, Basel, Switzerland. This article is an open access article distributed under the terms and conditions of the Creative Commons Attribution (CC BY) license (<https://creativecommons.org/licenses/by/4.0/>).

## 1. Introduction

The principles of fluid dynamics have long been used in competitive swimming to analyze performance and efficiency. In a sport where a spot on the podium can be determined by the length of a fingernail, it is no surprise that significant research and emphasis is placed on perfecting technique. A prominent example of the cutthroat nature of the sport was the men's 100 m butterfly final during the 2008 Beijing Olympics, where Michael Phelps out-touched Serbia's Milorad Cavic by 0.01 s [1].

Whether swimmers consciously realize it or not, the science of fluid dynamics plays at the heart of the sport, and technique is built around reducing the drag and maximizing thrust. It is of utmost importance for swimmers to consider technique from the perspective of drag minimization.

In swimming, drag is broadly categorized as either passive or active. Passive drag is drag for a swimmer in a stable position. For example, drag experienced by a swimmer during gliding (without kicking and pulling) is passive drag [2]. Active drag is resistance experienced by the swimmer when in dynamic motion. Active drag can be calculated

for swimmers performing one of the four strokes: freestyle, backstroke, breaststroke, and butterfly.

In this study, only passive drag is considered for the sake of simplicity; active drag introduces many complex factors due to the dynamic nature of swimming strokes and depends more on swim mechanics than shape [3]. This study explores the gliding phase in swimming, which occurs during the start and turns in the race and plays a crucial role in performance [2]. On average, the gliding phase contributes to approximately 10–15% of race time, and for breaststroke events it can be up to 44% of race time [4]. Specifically, the drag on the streamline, where the swimmer is in a prone position with arms extended at the front, is analyzed. Passive drag has a more direct relationship to body morphology, and analyzing the gliding phase is a good predictor of overall swimming performance.

### 1.1. Methods of Calculating Drag

In the past, there have been several methods used by coaches and scientists to analyze and calculate drag, including towing, flume, inverse dynamics, and computational fluid dynamics [5]. The first three mentioned are more experimentally based, using the motion and dynamics of the actual swimmer for calculations, while computational fluid dynamics simulates the swimmer moving through the water using modeling.

#### 1.1.1. Towing

One of the earliest methods used is towing, where drag force is directly calculated from a dynamometer, a device which measures force. Swimmers are attached to a towing cable and pulled through the water at specific velocities [5]. This is the most widely used and reliable method for calculating drag force.

#### 1.1.2. Flume

Similar to the towing method is the flume method. The swimmer is attached to a cable and water flows through the channel against the swimmer while he/she remains stationary. The drag force is measured in the same way as in towing [5]. One advantage to this method over towing is that the conditions are controlled and stable.

#### 1.1.3. Inverse Dynamics

This method uses the motion of the swimmer to determine the forces. This is typically performed on swimmers gliding off a push, and the change in velocity is used to measure the deceleration and the resistive force [5]. This method is convenient and economically advantageous.

#### 1.1.4. Computational Fluid Dynamics (CFD)

Computational fluid dynamics (CFD) is the most recently developed method out of the four. It typically uses a numerical (finite-element or finite volume) solver to calculate pressure and/or drag forces from a 2D or 3D model of a swimmer generated using fine mesh [5]. This method gives a detailed analysis of the fluid behavior around a swimmer, making it advantageous to use. Even though it inevitably produces numerical approximation errors, they can be minimized and controlled with a proper convergence analysis. Compared to other methods, CFD depends only on the generated model of the swimmer. Therefore, unwanted interference (factors that can lead to errors in experimental approaches) is not a concern with it [6]. This study employs only the CFD method.

In recent years, the computational fluid dynamic approach to calculating drag on a swimmer has become increasingly popular and reliable. It has been shown that CFD simulations on models generated by scanning swimmers obtained results within 4% of experimentally determined values [7].

The CFD method has been used in many different scenarios and has obtained useful results and insights. In one of the earliest studies, [6] analyzed just the swimmer's hand and arm at various angles. Later studies were done on the full body; two studies analyzed

the relationship between water depth on the drag coefficient during a streamline position at different velocities [2,8].

In this study, for simplicity and computational speed, we used 2D models for simulation. While 3D models could be more accurate, they would introduce many more variables and levels of complexity; 2D models are well established, and still offer a reliable and valid approach [9,10]. There have been many studies using 2D computational fluid dynamics simulations. Ref. [11] analyzed different streamline positions in breaststroke using the side-view projection. The lateral, dorsal, and prone positions in streamline were analyzed and compared. Another study analyzed the effects of gliding at free surface on flow characteristics using the side-view 2D projection as well [12]. Flow topography, turbulence, and pressure distribution were studied. In addition to measuring the effect of different positions on drag, some researchers also analyzed the effect of body shape on drag using computational fluid dynamics [13].

### *1.2. Impact of Morphology on Drag*

Because shape affects the drag coefficient [3], the morphology of swimmers has a great influence on hydrodynamics. Studies have found that body shape and structure do have a significant impact on resistance. Ref. [14] found that chest circumference and breadth, shoulder breadth, and height have an influence on passive drag. Another study analyzed the changes in body shape from pubertal development and found the correlation of anthropometric measurements with drag [15]. It was found that there was a difference between the drag of pre- and post-adolescent swimmers. Ref. [16] determined that morphology, characteristics such as fineness ratio and waist-to-hip taper index, has a bigger influence on drag and gliding performance than size. Ref. [13] studied differently shaped male bodies to analyze their hydrodynamic capabilities. Its result found that differently shaped torsos ranging from inverted triangular to rectangular resulted in varying drag forces, with the inverted triangle shaped experiencing the lowest drag. Both these studies found that larger chest-to-waist ratio and larger chest-to-hip ratio resulted in better gliding performance and lower drag coefficient. They imply that the shape of the swimmer's body has a noticeable effect on drag.

Most of the above studies had used the towing method and inverse dynamics (hydrokinematic) method. The main drawback of these methods is their inability to model and examine the exact behavior of flow. Flow characteristics can only be determined by observation and guesswork based on certain parameters. This study uses computational fluid dynamics to analyze the resistance (drag force) on swimmers as a function of their body shape (morphology).

### *1.3. Competitive Swimming and Sex Differences*

In the domain of competitive swimming, and in sports in general, it is well-noted that top male athletes predominantly perform better than female athletes.

According to [17], males swim 10% faster than females on average. This still holds up today, where the Olympic record for men in the 100 m freestyle is 9.6% faster than for women: 47.02 s set by Caeleb Dressel and 51.96 s by Emma McKeon at the 2020 Tokyo Games [18].

The gap in performance is attributed to several factors, including height, muscular mass, hormones, and fat distribution [17]. These lead to differences in power, endurance, and resistance. As a result of reaching puberty, males and females develop distinct body characteristics, such as changes in height and chest girth [15]. These differences in shape affects flow behavior and resistance [3]. Therefore, it is worth exploring if and to what extent there is a difference in drag between male and female swimmers.

### *1.4. Rationale*

A limited number of studies have analyzed the effects of morphological features on swim performance, and even fewer have done so using computational fluid dynamics [13].

There have also been a limited number of sources focusing on analyzing the difference between male and female drag coefficients as a result of shape. This study adds onto previous research done in morphology and swimming by exploring and quantifying the relationship between shape and the drag coefficient to determine whether female or male body types are better for gliding.

This study fills the gap in the knowledge of the effect of morphology on drag by using computational fluid dynamics (CFD) to analyze the behavior of flow around differently shaped swimmers, specifically with varying hip and chest sizes. It also improves upon previous 2D simulations by including a top (aerial) view projection of swimmers as well as the side view projection.

Analyzing and determining which body features have an effect on drag can help coaches find out what body shape is the most suitable for swimming. Our analysis can also influence the design of swim wear, compressing certain parts of the body to reduce drag.

We aim to quantify and analyze the effects of morphological factors on the drag coefficient and examine the case between male and female swimmers in a streamline position.

## 2. Theory

Fluid dynamics is the science of fluid motion and interaction. Therefore, understanding fluid dynamics is crucial for this study.

The behavior of fluids is mathematically described using the conservation of energy, momentum, and mass. For an incompressible fluid, the governing equations are as follows [19]:

$$\rho g_x - \frac{\partial P}{\partial x} + \mu \left( \frac{\partial^2 u}{\partial x^2} + \frac{\partial^2 u}{\partial y^2} + \frac{\partial^2 u}{\partial z^2} \right) = \rho \frac{Du}{Dt}, \quad (1)$$

$$\rho g_y - \frac{\partial P}{\partial y} + \mu \left( \frac{\partial^2 v}{\partial x^2} + \frac{\partial^2 v}{\partial y^2} + \frac{\partial^2 v}{\partial z^2} \right) = \rho \frac{Dv}{Dt}, \quad (2)$$

$$\rho g_z - \frac{\partial P}{\partial z} + \mu \left( \frac{\partial^2 w}{\partial x^2} + \frac{\partial^2 w}{\partial y^2} + \frac{\partial^2 w}{\partial z^2} \right) = \rho \frac{Dw}{Dt}, \quad (3)$$

$$\nabla \cdot V = 0 \quad (4)$$

where  $t$  is time,  $x$ ,  $y$ , and  $z$  are Cartesian spatial coordinates,  $\rho$  is density,  $g$  is gravitational constant,  $\mu$  is viscosity,  $P$  is pressure,  $V = \{u, v, w\}$  is the velocity vector, whereas  $u$ ,  $v$ , and  $w$  are its  $x$ ,  $y$ , and  $z$  components, respectively. The first three Equations (1)–(3) are known as the Navier–Stokes equations and describe the motion of fluid based on Newton’s 2nd Law of Motion. The last Equation (4) is a form of the continuity equation, derived from the conservation of mass.

### Drag

Drag exists as a result of pressure differences created by objects moving through a fluid. The pressure in the front of the moving object will be greater than the back, which creates a resistive force. There are two categories of drag: passive and active drag. Passive drag is resistance on a swimmer not in dynamic motion. For example, drag experienced by a swimmer during a streamline push-off without imparting forward thrust is passive drag force  $D_p$ :

$$D_p = \frac{C_d \rho A v^2}{2} \quad (5)$$

Where  $A$  is the frontal area of the swimmer,  $v$  is the velocity of the swimmer, and  $C_d$  is the drag coefficient of the swimmer. The drag coefficient is a dimensionless quantity dependent on shape, surface area, surface roughness, and flow characteristics indicating the level of hydrodynamic resistance [3].

Active drag is resistance on a swimmer considering both the resistive forces of the water and the propulsive forces of the swimmer. Because the frontal area and drag coeffi-

cient are constantly changing, calculating active drag is much more complicated [20]. To reducing complexity, only passive drag is considered in this study.

There are three types of drag which make up the total drag: frictional, pressure, and wave drag [3]. Frictional drag occurs at the boundary layer of the body, where the effects of viscosity are significant. The roughness of the surface slows the flow and creates a resistive force. Pressure drag is caused by a pressure difference between the front and rear of the body and is dependent on the frontal cross-sectional area and the shape of the swimmer. Wave drag is resistance from waves near the surface.

This study only considers frictional drag and pressure (form) drag, as at low depths, wave drag is negligible [2,11,13,21].

### 3. Materials and Methods

#### 3.1. Modeling the Swimmer

We consider two types of a 2D model of a swimmer: his/her side and top view. The models of male and female swimmers in both views are created using Microsoft Paint 3D software [22]. The same general model is used for each view (e.g., the side view female and side view male models were both created from the same model) to ensure consistency between the sexes. The models are drawn to match the average anthropometric measurements and proportions of males and females [23,24] as shown in Table 1. Namely, the arm length, leg length, torso length, hip depth and breadth, waist depth and breadth, and chest depth and breadth are proportioned to ensure that the models accurately represented typical male and female bodies, shown in Figures 1 and 2. Most notably, females have larger chest depths, hip depths, and hip breadths, while males have larger chest breadths. For analyzing certain body features and their effect on drag, the anthropometric measurements of the models are changed in increments, which is explained in more detail in the next section.

**Table 1.** Average Human Anthropometric Proportions (Percentage of Total Streamline Length) (From [23,24]).

|        | Leg Length (%) | Torso Length (%) | Arm Length (%) | Hip Breadth (%) | Hip Depth (%) | Waist Breadth (%) | Waist Depth (%) | Chest Breadth (%) <sup>1</sup> | Chest Depth (%) |
|--------|----------------|------------------|----------------|-----------------|---------------|-------------------|-----------------|--------------------------------|-----------------|
| Male   | 48.55          | 22.41            | 29.03          | 14.27           | 10.20         | 13.55             | 9.87            | 17.22                          | 10.53           |
| Female | 49.27          | 22.10            | 28.63          | 15.99           | 10.55         | 13.59             | 9.65            | 16.53                          | 11.21           |

<sup>1</sup> Measured from biacromial shoulder breadth.

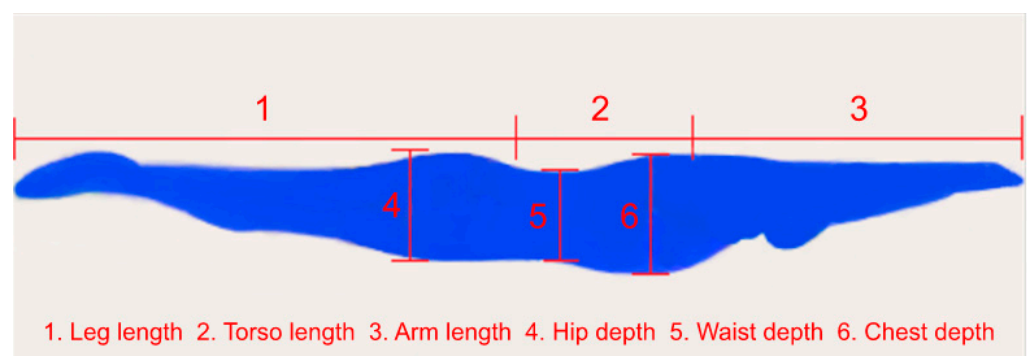
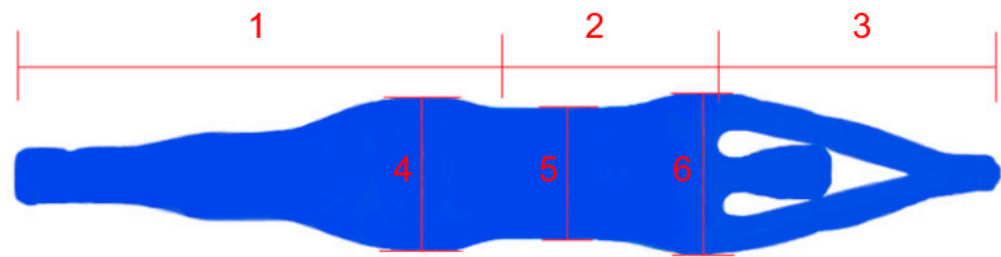


**Figure 1.** Anthropometric Features Measured on Female Side View Model.



1. Leg length 2. Torso length 3. Arm length 4. Hip breadth 5. Waist breadth 6. Chest breadth

**Figure 2.** Anthropometric Features Measured on Female Top View Model.

### 3.2. Resizing the Models

The models are initially sized such that the length of the female swimmer in streamline is set to be 2.2 m, based on the average height of male and female swimmers competing in the Olympics [25]. In order to ensure that size and height do not play an appreciable role in determining differences in drag in the simulations [14], the 2D model of the male swimmer is scaled down so that its streamline length is the same as that of the female swimmer: 2.2 m. The resizing is done while keeping the proportion of the body features the same.

### 3.3. Adapting and Importing the Models

Next an OpenCV algorithm [26] is used to trace the contour of the swimmers in streamline, and to write the coordinates of the contour (displayed in Figures 3 and 4 in green numbers) to a .txt file. The coordinates represent the points that define the shape of the contour used to recreate the original outline. After adjusting to realistically represent the swimmer and ensure the swimmers are in the same streamline position, the coordinates file is imported into Ansys Fluent and turned into a 2D curve.

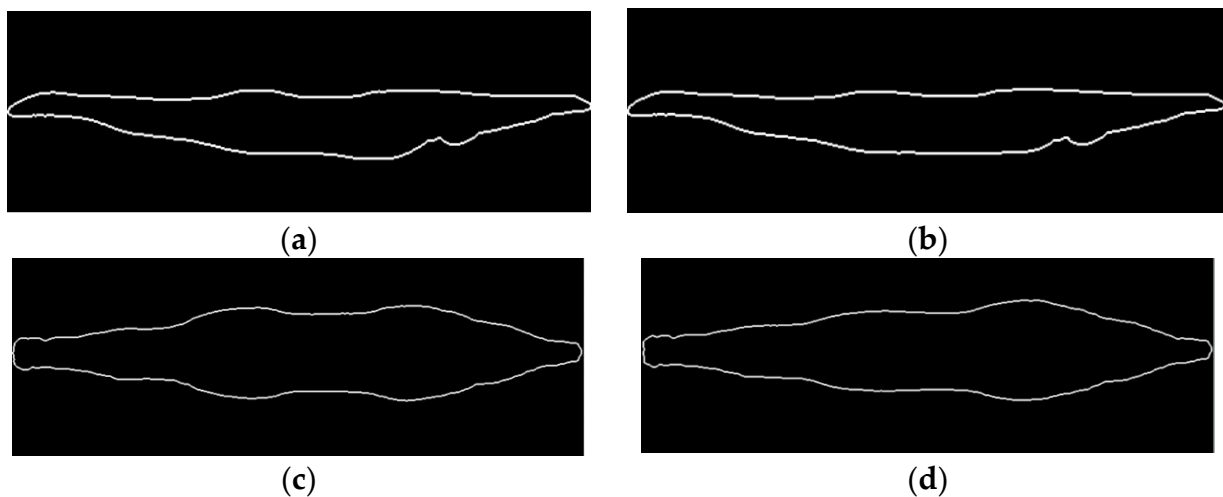


**Figure 3.** (a) Female Side View Contour; (b) Male Side View Model Contour; (c) Female Top View; (d) Male Top View.

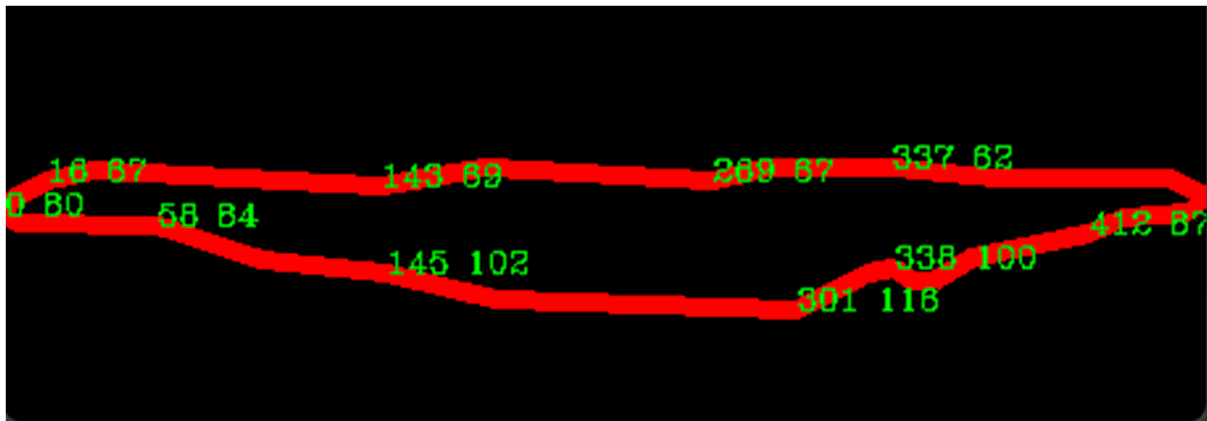


**Figure 4.** Contouring and Writing Coordinates (Displayed in green numbers, number of coordinates reduced for display clarity) for Female Side View Model.

### 3.4. Manipulating Anthropometry

To determine which and to what degree body features have an influence on the drag coefficient, the female side and top view models are manipulated by changing shape in several increments. Specifically, the hip region and chest/shoulder region are changed independently and analyzed. According to Table 1, these regions showed the greatest difference between sexes. Referencing Figures 1 and 2, the chest depth is calculated as the distance from the back to the bottommost point of the chest. The hip depth is calculated as the distance from the topmost point of the buttocks to the thigh. The hip breadth is calculated from the topmost to bottommost point of the hip, and the chest/shoulder breadth is calculated from the topmost to bottommost point of the trunk.

The chest and hip variables are changed relative to their original size (e.g., 5% increase in chest depth from the original measurement). For the side view female, the hip depth and chest depth are each changed by  $-10\%$ ,  $-7.5\%$ ,  $-5\%$ ,  $-2.5\%$ ,  $0\%$ ,  $2.5\%$ ,  $5\%$ ,  $7.5\%$ ,  $10\%$ . For the top view female, the hip breadth and chest breadth are also each changed by  $-10\%$ ,  $-7.5\%$ ,  $-5\%$ ,  $-2.5\%$ ,  $0\%$ ,  $2.5\%$ ,  $5\%$ ,  $7.5\%$ ,  $10\%$ . These relative changes were chosen to be within realistic human anthropometry. The hip and chest regions are changed independently (e.g., the hip is changed while keeping the rest of the model unchanged). The models are modified by manipulating the coordinates of the contours to obtain the desired measurements.

### 3.5. Computational Fluid Dynamics (CFD) and Computational Setup

Computational fluid dynamics (CFD) is a branch of fluid dynamics that uses numerical simulations to analyze and describe fluid flow and its interactions with solid bodies. The solutions to the Navier–Stokes and continuity equations can be found with a numerical solver to describe fluid behavior accurately and with detail. In this study, we use a CFD solver to analyze flow around a generated 2D model of a swimmer. We employ the standard k- $\omega$  turbulence model, as it was determined to be the best for capturing flow near the swimmer [27].

For our solver we use the commercially available Ansys Fluent CFD software, which uses the Finite Volume Method [28]. This is a well-established, thoroughly tested, and highly reliable software that originated in 1980s [29]. It has been successfully used in peer-reviewed studies by many researchers [30–32], including one of the authors of this paper [33], who also used the related software FIDAP, now owned by ANSYS as well [34].

For simplicity, we simulate the gliding phase of the swim (no kicking, no hand motions) in a coordinate system moving with the swimmer (or with a stationary swimmer in water flowing around him/her). To simulate a standard swimming pool, the computational domain is set up to be 8 m in length, and 1.83 m in depth. The water depth is in line with similar past studies, which have used depths of 1.5 m, 1.80 m, and 2.00 m [2,8,11–13].

The domain is then meshed the same for all simulations with finer mesh around the swimmer and boundaries (using 1013 divisions for the swimmer surface, 213 divisions for the inlet and outlet, and 356 divisions for the top and bottom surfaces, for a total of 25,055 cells), shown in Figure 5. To better capture flow around the swimmer, an inflation layer is established maintaining  $y^+$  values below 50 (non-dimensional distance measuring near-wall mesh resolution) on the surface of the swimmer [12].

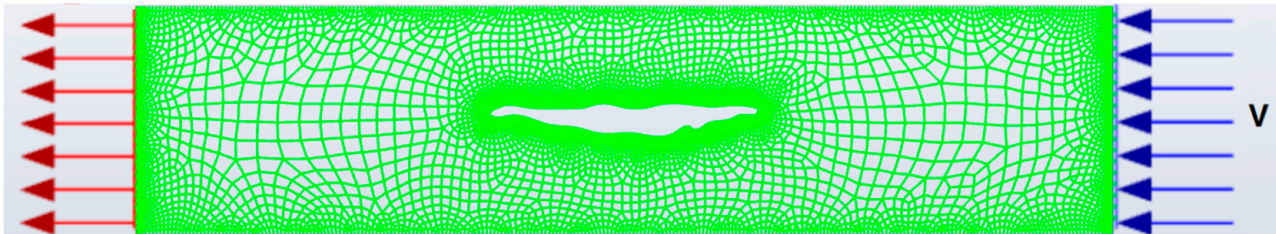


**Figure 5.** Computational Domain for Ansys Fluent Simulation (26,065 nodes, 25,055 cells).

The top and bottom of the domain are walls, and the inlet is on the side of the swimmer's hands and the outlet is on the side of the swimmer's feet. The swimmer is positioned at the center of the computational domain at a depth of 0.915 m, and there is interaction between the swimmer and the pool top and bottom. For the side view perspectives, 2D simulations in the vertical plane, the domain is considered between the surface and bottom of the pool with a slip condition (no shear stress) on the top and no-slip condition on the bottom walls. Due to negligible waves generated from gliding at the considered depth, the slip condition should suffice to model the free surface effects. For the top view perspectives, 2D simulations in the horizontal plane, the domain is considered to be the middle lane with slip conditions on the walls along the direction of the flow. Consequently, there are no free surface effects. For the wall condition of the swimmer, a no slip condition, a roughness height of 0, and a roughness constant of 0.5 is used. A convergence tolerance of  $1.0 \times 10^{-5}$  is also used.

### 3.6. Calculating Drag

The overall dimensions of the swimmer are needed for solving the 2D models. The front of the swimmer is defined to be the view when the swimmer is facing the observer and has the dimensions of width and depth.

The width and depth of the side view and top view models are determined to be accurate with average anthropometric measurements [23,24].

The frontal area is necessary for calculating the drag force and coefficient. The reference area, which is the frontal area inputted into the solver to calculate the drag coefficient from the drag force based on Equation (5), is calculated as an ellipse with depth and width as the ellipse axes:

$$A_{ref} = \frac{\pi}{4} \times depth \times width \quad (6)$$

This is done because it is more realistic than just multiplying the frontal dimensions. For the side and top views, the width is set to be the distance between the top and bottom most points/coordinates (as shown in Figure 4) of the swimmers. To complete the normalization of the male and female models, we give the side view models the same reference areas, and the top view models the same areas as well for the calculation of the drag coefficient. Thus, this makes a reasonable approximation for a meaningful comparison. Note that 3D modeling does not escape the issue of normalizing the male and female bodies. A more precise normalization can be investigated in the future.

The measurements relevant to the overall dimensions are different between male and female, resulting in different body shapes: the female chest depth is 6.5% greater than the resized male chest depth, the male shoulder breadth is 4.2% greater than the female



shoulder breadth, the female hip depth is 3.4% greater than the male hip depth, and the female hip breadth is 11.2% greater than the male hip breadth.

The density of water is set to  $998.2 \text{ kg/m}^3$ . The male and female models are tested for fluid velocities of 1.0, 1.5, 2.0, and 2.5 m/s, which translates to the reasonable range of Reynolds numbers from 200,000–1,000,000, considering biacromial shoulder width as the characteristic length. The models with changed anthropometry are tested for a velocity of 2.0 m/s. At the speeds and depths considered in this study, wave drag would contribute less than 5% of total drag and therefore is not considered [21].

These parameters are inputted into the solver for simulation.

### 3.7. Mesh Independence

To validate the results in this study, a mesh convergence test is performed. The convergence is demonstrated on the side female model shown in Table 2 and Figure 6. Because the results become independent for meshes with more than 25,000 cells, with a percent change of less than 1% from medium to fine mesh quality, the medium mesh resolution is used for the simulations to balance accuracy with computation time.

**Table 2.** Mesh Independence Study for Side View Female Model.

| Mesh Quality | Number of Cells | Drag Coefficient | Change (%) |
|--------------|-----------------|------------------|------------|
| Very Coarse  | 8173            | 0.2618           | N/A        |
| Coarse       | 17,515          | 0.2182           | 16.7       |
| Medium       | 25,055          | 0.2149           | 1.5        |
| Fine         | 36,696          | 0.2136           | 0.6        |

## Mesh Convergence Study

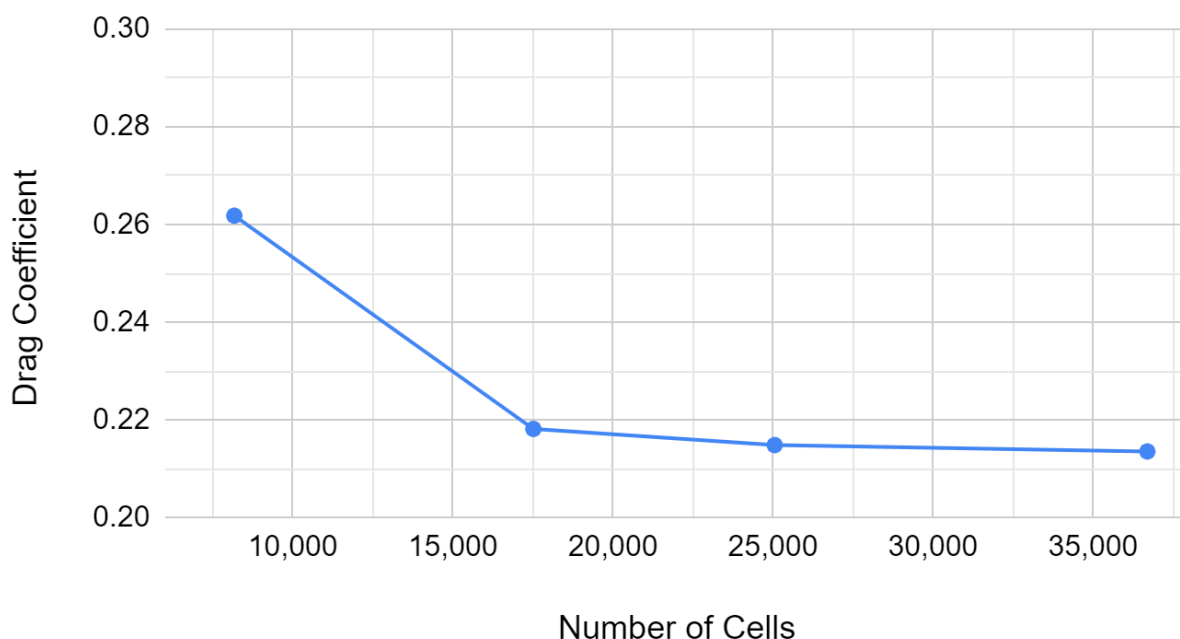


**Figure 6.** Graph of Mesh Convergence Study.

### 3.8. CFD Validation

The CFD simulations are validated by reproducing two published studies [9,10], measuring the drag coefficient of a cylinder, and comparing their results in Figures 7 and 8. The validation cases are very close to published numerical results. Therefore, the code and software are validated.

### Drag Coefficient vs. Reynolds Number: Son et al. (2020) vs Validation (Current Study)

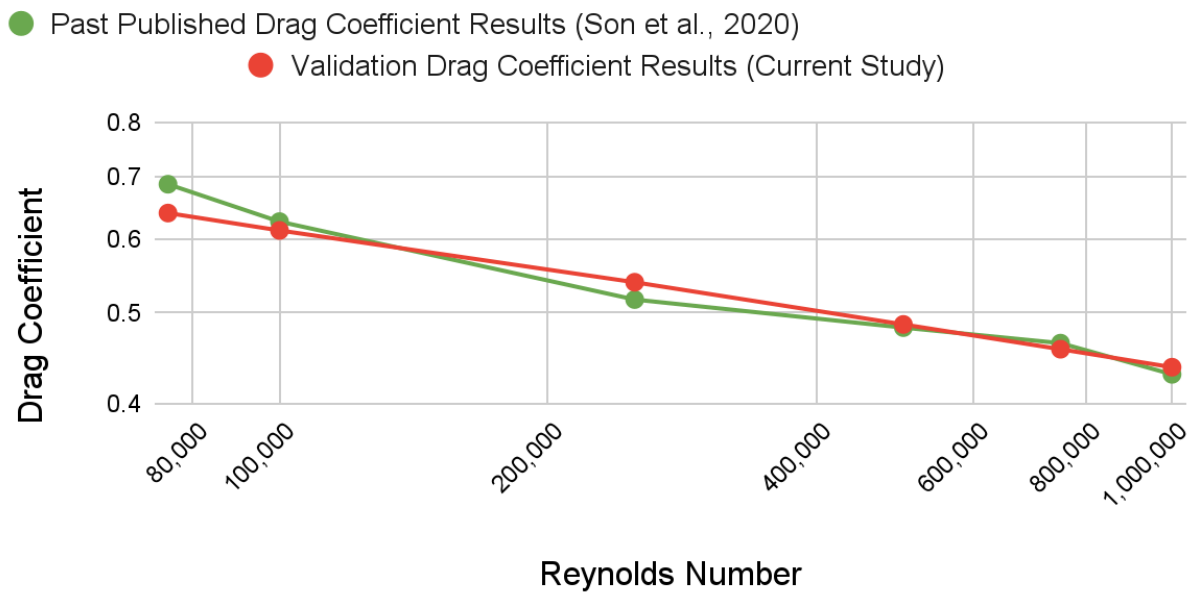


Figure 7. Graph Comparing Drag Coefficient Results: Son et al. [9] vs. Validation.

### Drag Coefficient vs. Reynolds Number: Yuce & Kareem (2016) vs Validation (Current Study)

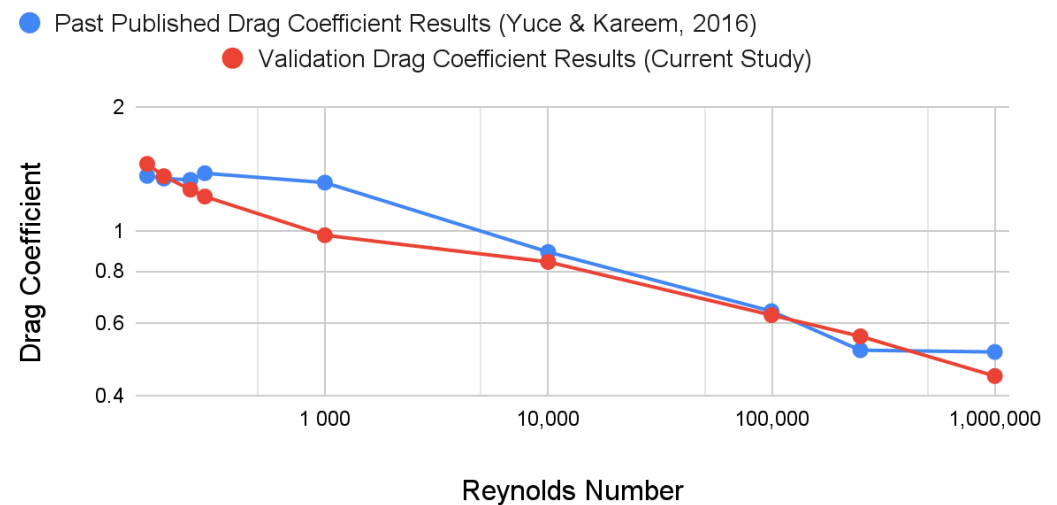


Figure 8. Graph Comparing Drag Coefficient Results: Yuce & Kareem [10] vs. Validation.

## 4. Results

### 4.1. Male and Female Comparison

We simulate 2D models of male and female swimmers in Ansys Fluent software at varying velocities. We created Tables 3 and 4 comparing the average drag forces and coefficients and Figures 9 and 10 comparing the models at different velocities.

**Table 3.** Average Drag Coefficients of 2D Models.

|                  | Average Pressure Drag Coefficient | Average Friction Drag Coefficient | Average Drag Coefficient |
|------------------|-----------------------------------|-----------------------------------|--------------------------|
| Male Side View   | 0.1399                            | 0.07407                           | 0.2140                   |
| Female Side View | 0.1471                            | 0.07369                           | 0.2207                   |
| Male Top View    | 0.1306                            | 0.05436                           | 0.1849                   |
| Female Top View  | 0.1529                            | 0.05218                           | 0.2051                   |

**Table 4.** Average Drag Forces of 2D Models.

|                  | Average Pressure Drag Force | Average Friction Drag Force | Average Drag Force |
|------------------|-----------------------------|-----------------------------|--------------------|
| Male Side View   | 17.05                       | 9.152                       | 26.19              |
| Female Side View | 17.84                       | 9.123                       | 26.96              |
| Male Top View    | 15.36                       | 6.639                       | 22.00              |
| Female Top View  | 18.08                       | 6.382                       | 24.46              |

### Drag Coefficients of 2D Models vs. Velocity

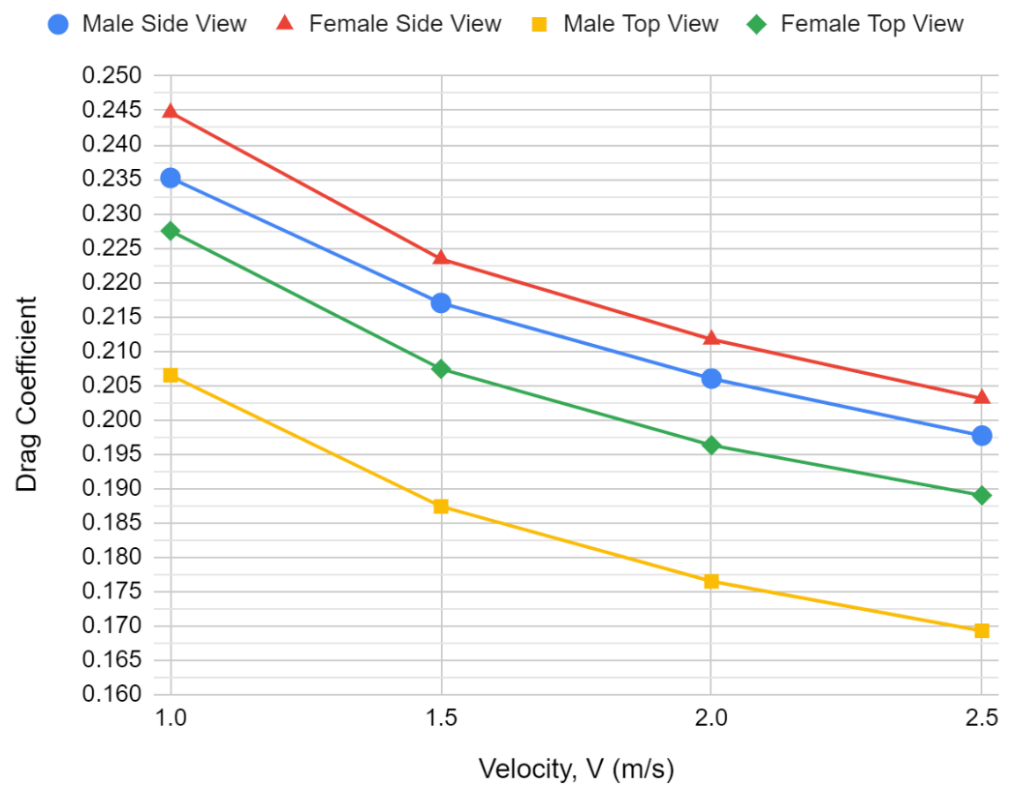


**Figure 9.** Graph of Drag Coefficients of 2D Models vs. Velocity (obtained from the drag force via Equation (5)).

### Drag Forces of 2D Models vs. Velocity

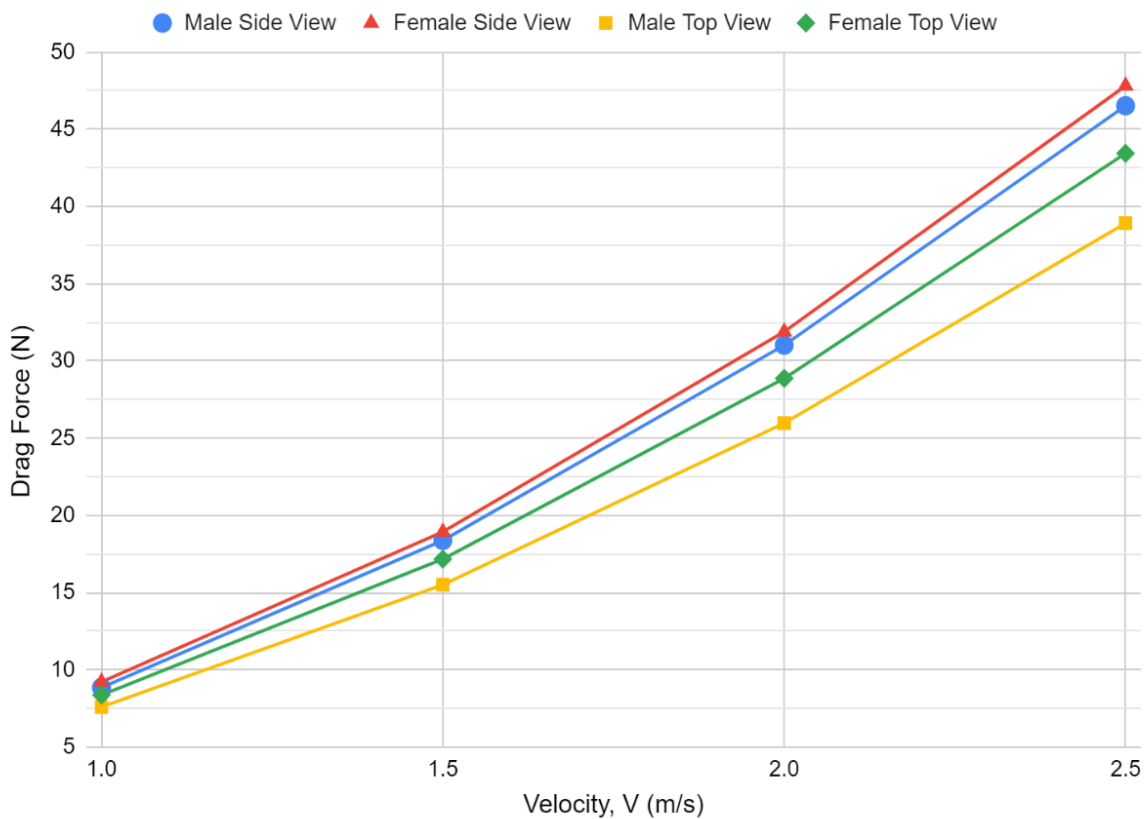


**Figure 10.** Graph of Drag Forces of 2D Models vs. Velocity.

#### 4.2. Manipulating Anthropometry

We simulate the female models with manipulated hip and chest variables at a velocity of 2 m/s. The results are in Figures 11–14 as follows:

### Drag Coefficient vs. Relative Hip Depth Change

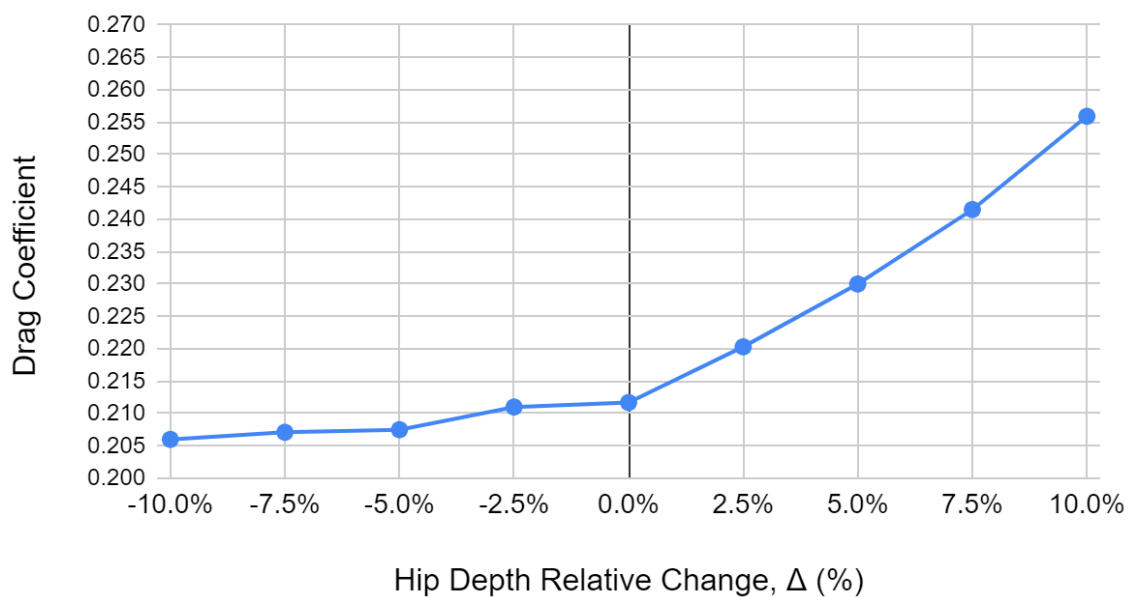


**Figure 11.** Graph of Relative Hip Depth Change (side view model) vs. Drag Coefficient.

### Drag Coefficient vs. Relative Chest Depth Change

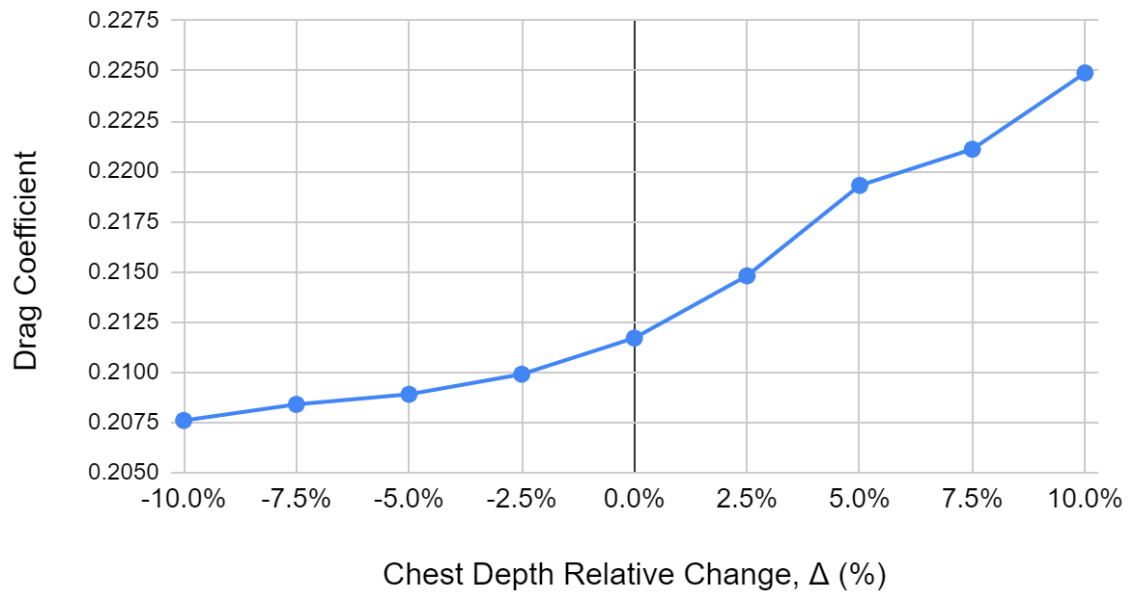


**Figure 12.** Graph of Relative Chest Depth Change (side view model) vs. Drag Coefficient.

### Drag Coefficient vs. Relative Hip Breadth Change

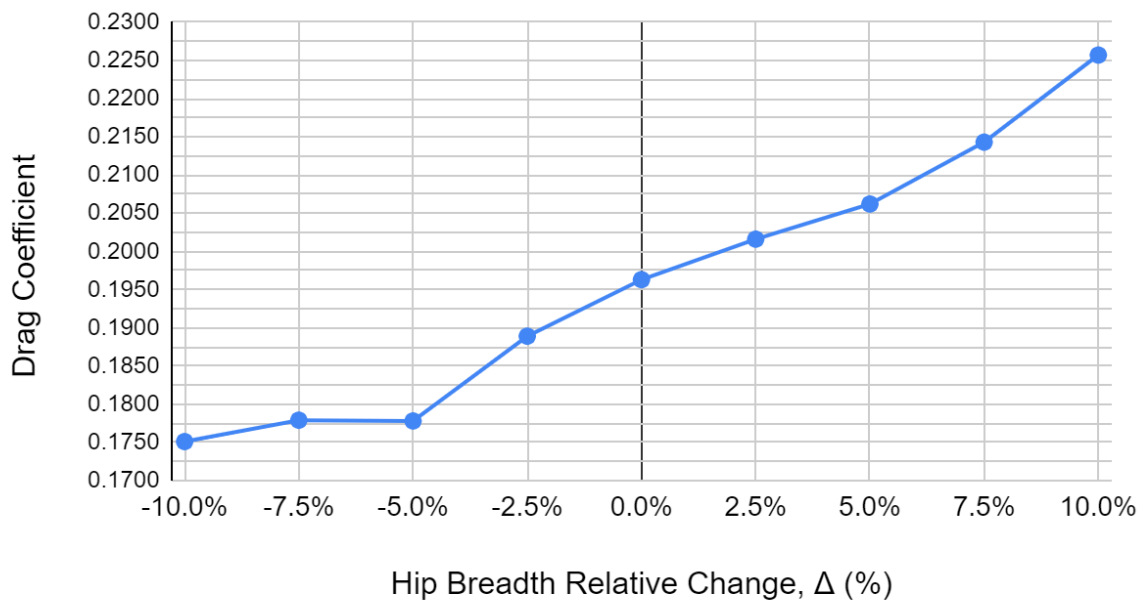


**Figure 13.** Graph of Relative Hip Breadth Change (top view model) vs. Drag Coefficient.

## Drag Coefficient vs. Relative Chest Breadth Change

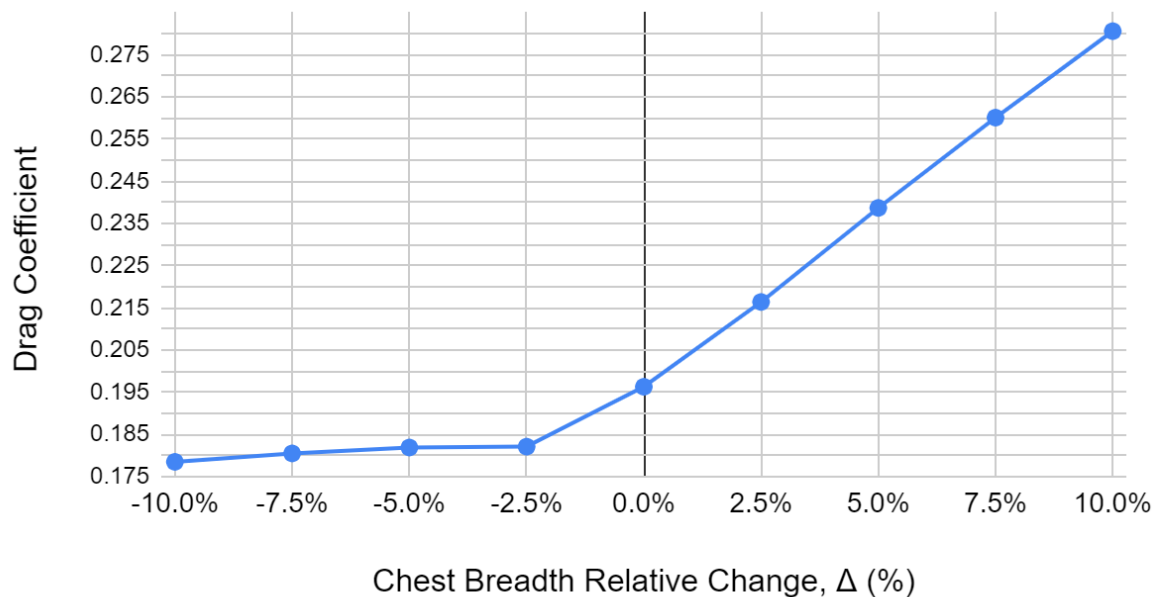


**Figure 14.** Graph of Relative Chest Breadth Change (top view model) vs. Drag Coefficient.

### 5. Discussion

The results reveal that there is a positive correlation between morphological factors and drag, specifically hip and chest size, and that the male body type is more hydrodynamic than the female body type.

#### 5.1. Drag Coefficient and Drag Force Sex Comparison

The drag force and coefficient of a male scaled down to female size are noticeably less than for a female. For the top view, the male drag coefficient on average is 10.1% lower than the female drag coefficient. For the side view, the male drag coefficient is 2.8% lower than the female drag coefficient. From the 2D simulations we conclude that a male swimmer is likely to outperform a female swimmer.

We note that the top view drag coefficient for males is significantly lower than the corresponding one for females, despite that the male frontal area is greater than the female due to a proportionally large shoulder breadth by 4%. This proves that the male top view has a more hydrodynamic shape and that the drag coefficient and “glide ability” is dependent more on shape than on size [16]. The side view male drag coefficient is also noticeably lower than the female drag coefficient. This can be attributed to both a larger female cross-sectional area and a more streamlined shape for the male.

In all simulations, we observe that the pressure drag force contributes to most of the total drag: on average 65.4% for side view male, 66.5% for side view female, 70.6% for top view male, and 74.6% for top view female. The top view model results are consistent with previous studies, which obtained percentages from 70–85% [7,13]. However, the side view models had a lower contribution of pressure drag.

Considering the individual contribution of pressure drag, there is a clear and consistent difference in sexes: the male models have lower pressure drag than females. However, for the friction drag coefficient, the male models for both side and top view have higher friction drag than the corresponding female models. The difference in drag between sexes is primarily a result of pressure drag, and the discrepancy in friction drag only has a small contribution.

There is a consistent trend between velocity and drag force: as velocity increases, the drag force increases. On the other hand, the drag coefficient and velocity have an inverse

relationship: as velocity increases, the drag coefficient slightly but consistently decreases. These relationships agree with past works [11,13].

Reinforced using multiple perspectives in the 2D simulations, the results show that the male body will experience less drag than the female body.

### 5.2. Anthropometry and Drag Coefficient Analysis

From the results of the simulations analyzing changes in body features, we conclude that the chest and hip region have a significant impact on the drag coefficient: as the chest and hip features increase in size, the drag coefficient increases as well. The graphs show an upward trend in the drag coefficient with an increase in the relative size of the targeted anthropometric measurements. Therefore, increasing hip or chest size, while keeping the other anthropometric measurements the same, magnifies drag.

We note that the drag coefficients for varying hip breadth and chest breadth have larger changes than for varying hip depth and chest depth: ranges of 0.20–0.26, 0.20–0.23, 0.17–0.23, and 0.17–0.28 for hip depth, chest depth, hip breadth, and chest breadth, respectively. This suggests that the breadth of a swimmer has a greater effect on drag than on depth. Referring to Figure 12, chest depth has a noticeably smaller influence on drag than the other parameters, with an average rate of change of 2.03% in drag force per 5% relative change. One plausible explanation is that the protruding head of the swimmer acts as a “buffer” for the flow against the curvature of the chest. Nonetheless, the results show that the chest depth changes still have significant effects on the drag. Drag because of varying hip depth has an average rate of change of 5.66% in drag force per 5% relative change. Hip breadth shows a relatively smaller average rate of change of 6.61% in drag force per 5% relative change than chest breadth. Chest breadth has the largest effect, with an average rate of change of 12.2% in drag force per 5% relative change. Similar for chest depth, an explanation for this is that the width of the trunk cushions the flow against the hip. These results are in line with past studies, which have shown experimentally that chest circumference and breadth have a significant impact on passive drag [3,14].

Another major observation consistent across all anthropometric features is that the drag coefficient changes taper off significantly as the relative size decrease. The positive relative anthropometric changes (2.5%, 5%, 7.5%, 10%) show much greater changes in drag coefficient than the negative changes (−2.5%, −5%, −7.5%, −10%). This suggests that drag is more sensitive to higher curvatures. One explanation is that lower curvature does not induce as much flow separation as increased curvature and irregular geometry [15]. Hence, any changes to a smaller curvature would have less of an effect on flow and drag [11]. Another explanation is that the lower curvature would expose other body features, increasing their impacts (e.g., the lower chest breadth would expose and increase the impact of the hips; the lower hip depth would expose the back of the legs). The less consistent trends in hip breadth, hip depth, and chest depth are likely because of complicated flow from interfering geometry, namely the swimmer’s trunk, back, and head.

Overall, we conclude that hip and chest size have a positive correlation with drag coefficients. In the context of sex comparison, these results explain why the male models outperform the female models and have lower drag. For the side view, the larger hip and chest depth contribute to the extra drag experienced by females. For the top view, while males have proportionally larger shoulder widths than females, their significantly smaller hip breadth lowers their drag. Past studies have shown that while chest circumference has a positive correlation with drag, the chest-to-waist ratio has a negative correlation with drag, meaning a higher chest-to-waist ratio, creating an “inverse triangular” shape, decreases drag [13,14,16]. The “inverse triangle” is closer to the “droplet” shape, which is the most hydrodynamic shape because it delays separation from the boundary layer because of its tapered profile [7]. Therefore, the “inverse triangular” shape and a higher chest-to-waist ratio are likely attributed to lowering the drag on male bodies [13,16].

These relationships between anthropometry and drag point to the fact that the male body shape is more hydrodynamic than the female body shape because of differences in the hip and chest.

### 5.3. Flow Analysis

We now examine the flow behavior through velocity vector visualization. The flow field for the female side view model simulated at a Reynolds number of 733,935, is shown in Figures 15 and 16. The analysis shows that there is flow separation and circulation zones in the regions around the neck and feet.

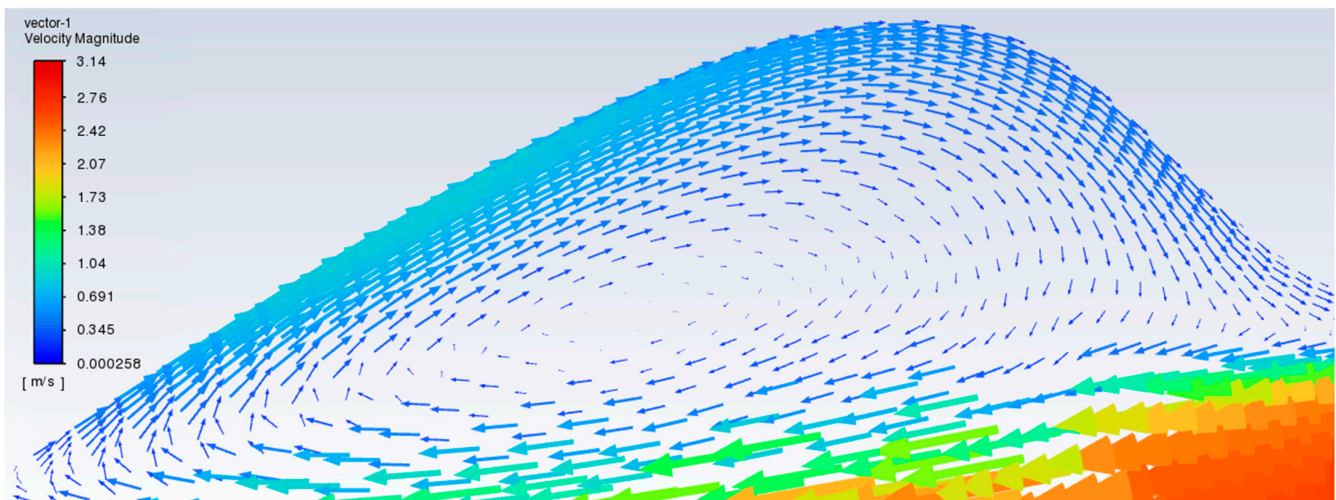


**Figure 15.** Flow Field Around Neck Region of Female Body from Side View.

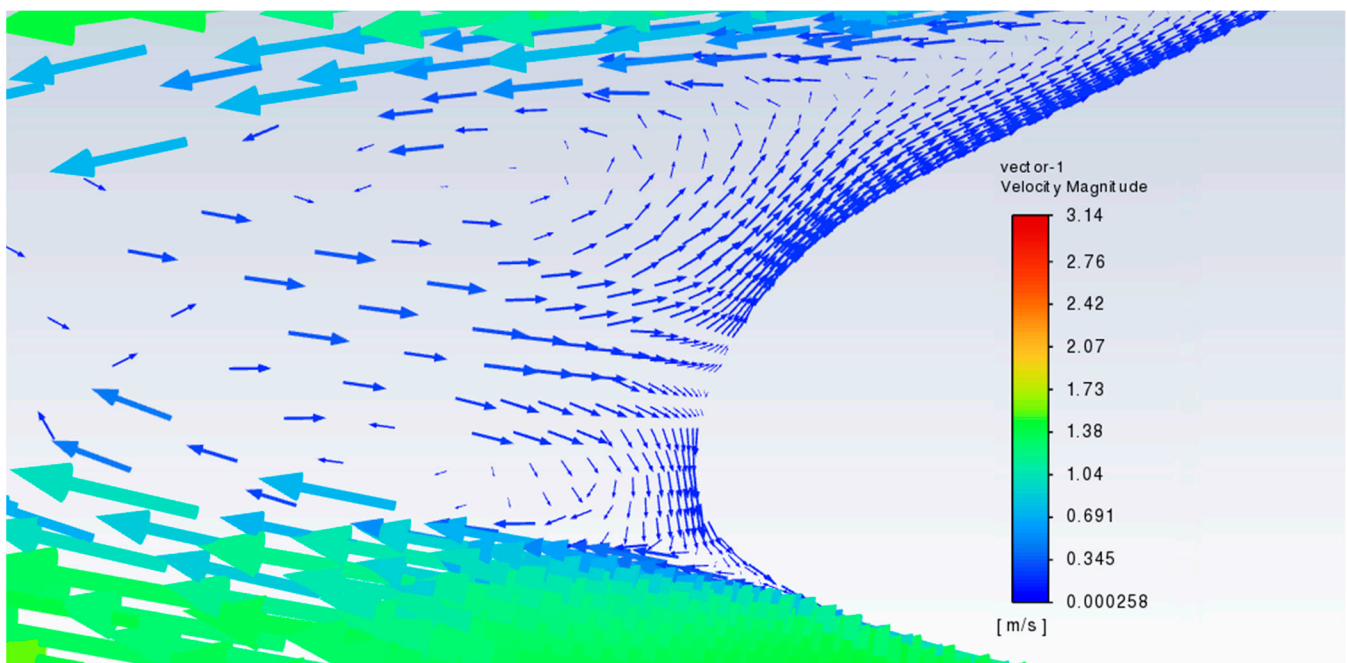


**Figure 16.** Flow Field Around Foot Region of Female Body from Side View.

### 5.4. Results Comparison

The overall drag forces obtained are close to, but lower than, the results from past studies using 2D and 3D simulations [7,11,13]. This study obtained drag forces in the range of 7.5–50 N for flow speeds of 1.0 to 2.5 m/s. The study in 2011 comparing different streamline positions found drag forces in the range of 30–80 N for flow speeds of 1.6 to



2.0 m/s. Another study in 2015 analyzing differently shaped torsos found drag forces on a range of 20–100 N for flow speeds of 1.2 to 2.2 m/s. A 2007 study comparing different methods of calculating drag found drag forces ranging from 30–70 N for flow speeds of 1.5 to 2.25 m/s.

The drag coefficient results deviate from those of past studies done with 3D simulations [7,13]. This study obtained coefficients in the range of 0.19–0.26. The 2015 study had a similar range of 0.28 to 0.36. The 2007 study also obtained close results, with the drag coefficient around 0.30 for flow speeds ranging from 1.5–2.25 m/s.

One explanation for the lower values is that the models are more streamlined than those in previous works; there are smoother surfaces and less protruding geometry. The lower values are also likely due to the inaccuracy of 2D simulations, which create unrealistic frontal areas for the models (the 2D models cannot capture the nuances in the depth “direction”) and miscalculate the drag force [5]. This study also does not simulate with the top of the domain open to air, which can lead to different flow behavior. Nonetheless, this does not impact the relative comparison between male and female drag.

The changes in drag because of anthropometric differences are like those found in [13]. We calculate from the 2015 study, which used 3D generated models of male swimmers, that a 5% increase in frontal area (chest circumference) and a 4.2% increase in hip size caused an average increase of 9.46% in drag force. In our study, a 5% increase in chest breadth and chest depth led to an average increase of 12.2% and 2.03% in drag force, respectively. A 5% increase in hip breadth and hip depth caused an average increase of 6.61% and 5.66%, respectively. The higher increase in drag force in the 2015 study is likely because multiple factors, hip size, waist size, and chest size, were changed simultaneously.

Overall, these results show that 2D simulations, while much simpler, can obtain realistic results consistent with 3D simulations.

##### 5.5. Differences in Drag on Swimming Performance

To consider how the changes in passive drag translate to performance at the competitive level, we compare the results from this study with the drag reduction effects of a swimmer wearing a *fastskin* suit, which is known to noticeably improve swim performance. [35] found a 7.7% reduction in passive drag for a full body *fastskin* suit compared to that of a normal suit. A later study determined that wearing a *fastskin* suit reduced passive drag by 6.2% and 4.7% for full body and waist-to-ankle suits, respectively, when compared to a normal suit [36]. The study also found that the overall performance improvement was a 3.2% and 1.8% decrease in time for the full body suit and waist-to-ankle suits, respectively. This supports a strong correlation between passive drag and swim performance found in [37]. The difference in drag forces between males and females in this study, 2.8% and 10.1% for side and top views, respectively, are comparable to the difference in drag forces between swimmers wearing *fastskin* suits and those that are not. Therefore, this suggests that the male body type has a significant performance advantage over the female body type.

## 6. Conclusions

We analyzed the impact of anthropometric features, specifically hip and chest size, on drag and compared 2D models of male and female swimmers. The simulations show that the morphology of a normalized male body results in a more hydrodynamic profile than that of a female body, showing differences of 2.8% and 10.1% in drag, and determine that hip and chest size play significant roles in drag, with a large 12.2% change in drag per 5% change in chest breadth. These drag differences between males and females are proven to be significant for performance by comparing them to drag differences of 6.2% and 7.7% between *fastskin* and normal suits. These results contribute to the body of knowledge in human engineering and biomechanics. This study has shown that purely from a body structure standpoint, swimmers with a male body type have an advantage over swimmers with a female body type. Additionally, this difference, again, is comparable to the difference in drag forces between swimmers who do wear *fastskin* suits and those who do not.

This study builds on other related works by using computational fluid dynamics (CFD) to analyze in detail the fluid behavior around swimmers with varying body shapes, offering a more theoretical approach. It provides a more in-depth analysis by quantifying how changing different morphological features affects drag. It also simulates a top view projection, adding a different perspective to 2D simulations, which reinforces the results. The benefits of our approach are its simplicity and effectiveness. It builds a solid foundation for future investigation in the application of CFD to competitive swimming.

#### *Future Research*

Several changes/additions can be made for improvement. In the future, athletic body morphology should be considered; this study uses the morphology based on average statistics, so it does not give an ideal representation of a swimmer body. Future works may analyze how other morphological factors, such as chest-to-waist ratio, hip-to-waist ratio, and arm/leg/torso length, affect drag. Other additions/changes include the consideration of active drag, which involves body movement of the swimmer. Free-surface effects and analysis of wave drag [21] can also be considered. To study a realistic pool environment, the wave interaction between multiple swimmers should be examined [38]. Furthermore, studies can use 3D models for more accurate simulations, as opposed to 2D. This study uses unstructured grids for numerical simulation; future studies simulating fluid flow with a deformable body (i.e., simulating moving limbs and skin deformation) should use the immersed boundary method [39,40]. Comparing the energy cost of swimming for males and females, in addition to body structure, is another consideration to advance the field of human swimming. Finally, while this study and many others perform CFD simulations on unstructured grids, an alternative venue is the immersed boundary method. This technique proves to be viable for flexible and deforming structures, applicable to dynamic motion of swimmers that can be explored in future research [39,40].

These results can influence the future design of swimwear to minimize drag and help coaches, swimmers, and researchers find the ideal swimmer body type.

**Author Contributions:** Conceptualization, Data analysis, Methodology, Software selection, Validation/Convergence analysis, Writing—review and editing: A.X.G.W. and Z.J.K.; Simulations, Visualization, Writing—original draft: A.X.G.W.; Supervision: Z.J.K. All authors have read and agreed to the published version of the manuscript.

**Funding:** This research received no external funding.

**Institutional Review Board Statement:** Not applicable.

**Informed Consent Statement:** Not applicable.

**Data Availability Statement:** Fluent simulation data files are available upon request.

**Acknowledgments:** We would like to express our gratitude to two anonymous reviewers, who provided an in-depth constructive critique and suggestions for improving this manuscript. We are also grateful to the editorial staff for professional and efficient handling of our paper.

**Conflicts of Interest:** The authors declare no conflict of interest.

#### **References**

1. Wei, T.; Mark, R.; Hutchison, S. The Fluid Dynamics of Competitive Swimming. *Annu. Rev. Fluid Mech.* **2014**, *46*, 547–565. [[CrossRef](#)]
2. Novais, M.; Silva, A.; Mantha, V.; Ramos, R.; Rouboa, A.; Vilas-Boas, J.P.; Luís, S.; Marinho, D. The Effect of Depth on Drag During the Streamlined Glide: A Three-Dimensional CFD Analysis. *J. Hum. Kinet.* **2012**, *33*, 55–62. [[CrossRef](#)] [[PubMed](#)]
3. Naemi, R.; Easson, W.J.; Sanders, R.H. Hydrodynamic glide efficiency in swimming. *J. Sci. Med. Sport* **2010**, *13*, 444–451. [[CrossRef](#)] [[PubMed](#)]
4. Vilas-Boas, J.P.; Costa, L.; Fernandes, R.J.; Ribeiro, J.; Figueiredo, P.; Marinho, D.; Silva, A.J.; Rouboa, A.; Machado, L. Determination of the Drag Coefficient during the First and Second Gliding Positions of the Breaststroke Underwater Stroke. *J. Appl. Biomech.* **2010**, *26*, 324–331. [[CrossRef](#)]

5. Scurati, R.; Gatta, G.; Michielon, G.; Cortesi, M. Techniques and considerations for monitoring swimmers' passive drag. *J. Sports Sci.* **2018**, *37*, 1168–1180. [CrossRef]
6. Bixler, B.; Riewald, S. Analysis of a swimmer's hand and arm in steady flow conditions using computational fluid dynamics. *J. Biomech.* **2002**, *35*, 713–717. [CrossRef]
7. Bixler, B.; Pease, D.; Fairhurst, F. The accuracy of computational fluid dynamics analysis of the passive drag of a male swimmer. *Sports Biomech.* **2007**, *6*, 81–98. [CrossRef]
8. Mantha, V.R.; Marinho, D.A.; Silva, A.J.; Rouboa, A. The 3D CFD study of gliding swimmer on passive hydrodynamics drag. *Braz. Arch. Biol. Technol.* **2014**, *57*, 302–308. [CrossRef]
9. Son, H.A.; Lee, S.; Lee, J. Numerical Analysis of Drag Force Acting on 2D Cylinder Immersed in Accelerated Flow. *Water* **2020**, *12*, 1790. [CrossRef]
10. Yuce, M.I.; Kareem, D.A. A Numerical Analysis of Fluid Flow Around Circular and Square Cylinders. *J. Am. Water Work. Assoc.* **2016**, *108*, E546–E554. [CrossRef]
11. Marinho, D.; Barbosa, T.; Rouboa, A.; Silva, A. The Hydrodynamic Study of the Swimming Gliding: A Two-Dimensional Computational Fluid Dynamics (CFD) Analysis. *J. Hum. Kinet.* **2011**, *29*, 49–57. [CrossRef] [PubMed]
12. Hayati, A.N.; Ghaffari, H.; Shams, M. Analysis of free-surface effects on swimming by the application of the computational fluid dynamics method. *Proc. Inst. Mech. Eng. Part P J. Sports Eng. Technol.* **2016**, *230*, 135–148. [CrossRef]
13. Li, T.-Z.; Zhan, J.-M. Hydrodynamic body shape analysis and their impact on swimming performance. *Acta Bioeng. Biomech.* **2015**, *17*, 3–13. [PubMed]
14. Cortesi, M.; Gatta, G.; Michielon, G.; di Michele, R.; Bartolomei, S.; Scurati, R. Passive Drag in Young Swimmers: Effects of Body Composition, Morphology and Gliding Position. *Int. J. Environ. Res. Public Health* **2020**, *17*, 2002. [CrossRef] [PubMed]
15. Benjanuvatra, N.; Blanksby, B.A.; Elliott, B.C. Morphology and Hydrodynamic Resistance in Young Swimmers. *Pediatr. Exerc. Sci.* **2001**, *13*, 246–255. [CrossRef]
16. Naemi, R.; Psycharakis, S.G.; McCabe, C.; Connaboy, C.; Sanders, R.H. Relationships Between Glide Efficiency and Swimmers' Size and Shape Characteristics. *J. Appl. Biomech.* **2012**, *28*, 400–411. [CrossRef] [PubMed]
17. Thibault, V.; Guillaume, M.; Berthelot, G.; Helou, N.E.; Schaal, K.; Quinquis, L.; Nassif, H.; Tafflet, M.; Escolano, S.; Hermine, O.; et al. Women and Men in Sport Performance: The Gender Gap has not Evolved since 1983. *J. Sports Sci. Med.* **2010**, *9*, 214–223.
18. Divers, S.S. How Fast Do Olympic Swimmers Swim? Men vs. Women vs. Average Swimmers. Triathlon Budgeting. 2021. Available online: <https://triathlonbudgeting.com/how-fast-do-olympic-swimmers-swim-men-vs-women-vs-average-swimmers> (accessed on 14 July 2022).
19. Kleinstreuer, C. Fundamental Equations and Solutions. In *Fluid Mechanics and Its Applications*; Springer: Berlin/Heidelberg, Germany, 2010; pp. 41–98. [CrossRef]
20. Gatta, G.; Cortesi, M.; Fantozzi, S.; Zamparo, P. Planimetric frontal area in the four swimming strokes: Implications for drag, energetics and speed. *Hum. Mov. Sci.* **2015**, *39*, 41–54. [CrossRef]
21. Vennell, R.; Pease, D.; Wilson, B. Wave drag on human swimmers. *J. Biomech.* **2006**, *39*, 664–671. [CrossRef] [PubMed]
22. Microsoft Corporation. Get Paint 3D from the Microsoft Store. Microsoft Apps. 2022. Available online: <https://apps.microsoft.com/store/detail/paint-3d/9NBLGGH5FV99?hl=en-us&gl=US> (accessed on 2 August 2022).
23. Anthropometric Data for U.S. Adults (All Dimensions in Inches). 2012. Available online: <https://www.ergocenter.ncsu.edu/wp-content/uploads/sites/18/2017/09/Antropometric-Summary-Data-Tables.pdf> (accessed on 14 July 2022).
24. Ergonomics—Army Public Health Center. 2012. Available online: <https://phc.amedd.army.mil/topics/workplacehealth/ergo/Pages/default.aspx> (accessed on 14 July 2022).
25. Madge, R. Height Analysis of Rio Swimming Finalists. *Swimming World News*, 24 August 2016. Available online: <https://www.swimmingworldmagazine.com/news/height-analysis-of-rio-swimming-finalists> (accessed on 14 July 2022).
26. Find Co-Ordinates of Contours Using OpenCV: Python. GeeksforGeeks. 2019. Available online: <https://www.geeksforgeeks.org/find-co-ordinates-of-contours-using-opencv-python/> (accessed on 1 August 2022).
27. Zaidi, H.; Fohanno, S.; Taiar, R.; Polidori, G. Turbulence model choice for the calculation of drag forces when using the CFD method. *J. Biomech.* **2010**, *43*, 405–411. [CrossRef] [PubMed]
28. ANSYS, Inc. Ansys Fluent | Fluid Simulation Software. 2022. Available online: <https://www.ansys.com/products/fluids/ansys-fluent> (accessed on 2 August 2022).
29. Analysis Origins—Fluent, 2019. National Agency for Finite Element Methods and Standards (NAFEMS). Available online: <https://www.nafems.org/blog/posts/analysis-origins-fluent/> (accessed on 22 August 2022).
30. Greifzu, F.; Kratzsch, C.; Forgber, T.; Lindner, F.; Schwarze, R. Assessment of particle-tracking models for dispersed particle-laden flows implemented in OpenFOAM and ANSYS FLUENT. *Eng. Appl. Comput. Fluid Mech.* **2015**, *10*, 30–43. [CrossRef]
31. Hosseini, S.; Tafreshi, H.V. Modeling particle-loaded single fiber efficiency and fiber drag using ANSYS-Fluent CFD code. *Comput. Fluids* **2012**, *66*, 157–166. [CrossRef]
32. Nair, A.S.; Mathew, M.P. *Resistance Estimation of Ships Using GEKO Turbulence Model in ANSYS Fluent*; IEEE: Manhattan, NY, USA, 2022; pp. 1–9. [CrossRef]
33. Kabala, Z.J.; Kim, Y.W. Dynamic Effective Porosity: Numerical Simulations. *J. Res. Inst. Eng. Technol.* **2011**, *30*, 91–95.
34. Kahler, D.M.; Kabala, Z.J. Acceleration of groundwater remediation by deep sweeps and vortex ejections induced by rapidly pulsed pumping. *Water Resour. Res.* **2016**, *52*, 3930–3940. [CrossRef]

35. Benjanuvatva, N.; Dawson, G.; Blanksby, B.; Elliott, B. Comparison of buoyancy, passive and net active drag forces between Fastskin™ and standard swimsuits. *J. Sci. Med. Sport* **2002**, *5*, 115–123. [[CrossRef](#)]
36. Chatard, J.-C.; Wilson, B. Effect of Fastskin Suits on Performance, Drag, and Energy Cost of Swimming. *Med. Sci. Sports Exerc.* **2008**, *40*, 1149–1154. [[CrossRef](#)] [[PubMed](#)]
37. Chatard, J.-C.; Bourgoin, B.; Lacour, J.R. Passive drag is still a good evaluator of swimming aptitude. *Eur. J. Appl. Physiol. Occup. Physiol.* **1990**, *59*, 399–404. [[CrossRef](#)]
38. Yuan, Z.-M.; Li, M.; Ji, C.-Y.; Li, L.; Jia, L.; Incecik, A. Steady hydrodynamic interaction between human swimmers. *J. R. Soc. Interface* **2019**, *16*, 20180768. [[CrossRef](#)]
39. Afra, B.; Nazari, M.; Kayhani, M.; Delouei, A.A.; Ahmadi, G. An immersed boundary-lattice Boltzmann method combined with a robust lattice spring model for solving flow–structure interaction problems. *Appl. Math. Model.* **2018**, *55*, 502–521. [[CrossRef](#)]
40. Afra, B.; Karimnejad, S.; Delouei, A.A.; Tarokh, A. Flow control of two tandem cylinders by a highly flexible filament: Lattice spring IB-LBM. *Ocean Eng.* **2022**, *250*, 111025. [[CrossRef](#)]